

Article

Effect of Laminar Flow on the Corrosion Activity of AA6061-T6 in Seawater

Gloria Acosta ¹, Lucien Veleva ^{1,*} , Luis Chávez ¹ and Juan L. López ² 

¹ Applied Physics Department, Research Center for Advanced Study (CINVESTAV-IPN), Mérida 97310, Mexico; glori_acosta@hotmail.com (G.A.); luis.chavez@cinvestav.mx (L.C.)

² Centro de Innovación en Ingeniería Aplicada, Universidad Católica del Maule, Talca 3460000, Chile; jlopez@ucm.cl

* Correspondence: veleva@cinvestav.mx; Tel.: +52-999-942-9400

Received: 17 December 2019; Accepted: 21 January 2020; Published: 24 January 2020



Abstract: The electrochemical behaviour and surface changes on AA6061-T6 alloy exposed to Caribbean seawater from the Cozumel Channel for 30 days under laminar flow (0.1 m s^{-1}) were studied, contrasting then with stationary (no flow) conditions. Monitoring of open-circuit potential and current fluctuations, both considered as electrochemical noise (EN), were employed as two nondestructive methods. The calculated corrosion current, based on R_n , was one order higher in laminar flow. The fluctuations of current were transformed in the frequency domain. Their power spectral density (PSD) plots were obtained in order to gain information concerning the dynamic of the spontaneous release of energy during the corrosion process. The value of the exponent β in PSD graphs suggested that the localised corrosion on AA6061-T6 surface occurs as a persistent stationary process, in which dynamic is controlled by oxygen diffusion and its renewal at the metal interface. The changes in the morphology and elemental composition of the formed layers revealed that the localized attacks occurred in the vicinity of intermetallic particles rich in Fe and Cu, which act as cathodes.

Keywords: aluminum alloy 6061-T6; seawater; laminar flow; intermetallic particles; electrochemical noise

1. Introduction

Aluminum alloy (AA) 6061-T6 is popular as a nonferrous material for structures in seawater [1] and is characterised by various properties, such as strength-to-weight ratio, extrudability—particularly for the manufacture of profiles with complex geometry—low thermal expansion coefficient, good wear resistance, and corrosion resistance [2]. The alloy presents good corrosion resistance in many environments having neutral pH because of the formation of a protective amorphous aluminum oxide film on its surface of approximately 2–3 nm thickness and its insolubility in water [3,4]. The addition of alloying elements to aluminum increases its mechanical properties [5]; however, the precipitated intermetallic particles (IMPs) have a harmful effect on the corrosion resistance of the Al alloys [4,6–11]. IMPs present electrochemical behaviour different from the alloy matrix, and they may be classified in two types: cathodic and anodic [7,9–13]. The electrochemically active anodic particles are rich in Mg, Si, and Al, with Mg preferential dissolution, leaving a cavity in the oxide layer, while the cathodic particles are rich in Fe, Si, and Cr, acting as preferential sites for oxygen reduction.

The localised corrosion becomes greater in the presence of aggressive ions, such as chlorides [4,14–16], and corrosion pits initiate in oxide film sites, weakened by chloride attack. Moreover, the heterogeneity of the surface could result in favourable nucleation sites.

Seawater is a complex electrolyte of different ions, with a high salinity (3.5 wt.%, density 1.023 g/cm^3 at $25 \text{ }^\circ\text{C}$), which causes damage to metals in a short time [17,18]. The principal parameters

that affect the corrosion behaviour of metals immersed in this electrolyte are oxygen content, dissolved mineral salts, pH, temperature, specific contaminants, and flow velocity [17,19].

The characterisation of the corrosion process requires electrochemical nondestructive techniques, and preferred methods are those that do not apply external polarization. The monitoring of the open circuit potential (φ_{corr} , free corrosion potential) or corrosion current is one of these and is easy to handle. Fluctuations may be interpreted as electrochemical noise (EN), which is a useful for the purposes of corrosion mechanism characterization. Electrochemical noise is presented by random fluctuations of corrosion potential or current, typically with frequencies below 10 Hz and with low amplitude [20]. This technique can provide information concerning the nature of the corrosion process and the rate thereof. The main sources of EN observed in corrosion systems are attributed to microscopic and macroscopic events [20–22]. EN measurements can be performed under corrosion potential or any constant potential/current, depending on the research objective, to analyse the corrosion mechanism and to obtain the corrosion rate [21].

EN measurements can be analysed by transforming the data in the frequency domain by fast Fourier transform (FFT) to obtain power spectral density (PSD) [23,24]. PSD plots display a slope, β exponent, which enables differentiation between series with fractional Gaussian noise (fGn , β from -1 to 1) and fractional Brownian motion (fBm , β from 1 to 3). The fGn is a stationary process and the fBm is nonstationary [25,26]. The β exponent is a parameter correlated with the strength of persistence in a process [27]. In our previous studies, EN technique was carried out to characterize the first stages of corrosion in stationary seawater of copper [28], aluminum [29], and aluminum alloys [30] as well as the initial stages of AZ31B Mg alloy in simulated body fluid [31].

The object of this study is to investigate the electrochemical behaviour and surface changes on AA6061-T6 alloy exposed to Caribbean seawater (Cozumel Channel) under laminar flow, contrasting these with stationary flow. Two nondestructive electrochemical methods were used to test the corrosion resistance of the alloy. The corrosion current and φ_{corr} were considered as EN and transformed in the frequency domain in order to gain information on the dynamics of the spontaneous release of energy during the corrosion process. X-ray photoelectron spectroscopy (XPS) measurement was employed to analyse the composition of the formed corrosion layers, as well as SEM-EDS surface analysis. To the best of the authors' knowledge, there is still no study on the initial stages of localised corrosion of AA6061-T6 alloy in laminar flow conditions.

2. Materials and Methods

The nominal composition of AA6061-T6 (Metal Plastic Mexicali) was (wt.%) 1.10% Mg, 0.5% Fe, 0.4% Si, 0.31% Cu, 0.19% Cr, 0.07% Zn, 0.05% Ti, and the remainder Al. The seawater was extracted from the Caribbean Cozumel Channel at 10 km offshore to minimize the effect of human pollution and at a depth of 10 m. The seawater composition and physicochemical properties were as follows: salinity 36.4 g L^{-1} , chlorides 20.12 g L^{-1} , sulfates 2.82 g L^{-1} , nitrates $0.48 \text{ } \mu\text{mol L}^{-1}$, nitrites $0.18 \text{ } \mu\text{mol L}^{-1}$, ammonia $0.99 \text{ } \mu\text{mol L}^{-1}$, pH 7.3, dissolved oxygen 5.8 mg L^{-1} , and conductivity 51.6 mS .

Samples of 1 cm^2 were embedded in Epofix resin as working electrodes for electrochemical tests. In addition, samples of 1 cm^2 were cleaned with ethanol and immersed in 100 mL of seawater (triplicated) under flow conditions for 0, 5, 15, and 30 days. Before exposure, the specimens were ground with silicon carbide paper to 4000 grit, using distilled water as lubricant. They were washed with distilled water and dried in air.

2.1. Laminar Flow of Seawater

The speed range found in the Cozumel Channel indicates that the ocean current speed oscillates between 0.1 m s^{-1} to 1 m s^{-1} . The tubing employed to connect the peristaltic pump (LAMBDA Laboratory Instrument) with the electrochemical cell has a diameter of 6 mm, and using the lower limit of the flow speed (0.1 m s^{-1}), the calculated Reynolds number was 622.97, which corresponds to

laminar hydrodynamic flow [32]. The dimensionless N_{Re} characterises the diffusion-dependent system and is governed by the ratio of the inertial forces acting on the fluid to the viscous forces:

$$N_{Re} = \frac{\rho \bar{u} d}{\mu} \quad (1)$$

where ρ is the fluid density (seawater: 997.8 kg m^{-3}), \bar{u} is the flow speed (0.1 m s^{-1}), d is the tubing diameter (6 mm), and μ is the seawater viscosity ($0.961 \times 10^{-3} \text{ N s m}^{-2}$). All experiments were carried out at $21 \text{ }^\circ\text{C}$.

2.2. Surface Analysis

AA6061-T6 samples were characterised before and after exposure in seawater by SEM-EDS (Phillips-XL30, Phillips, Amsterdam, The Netherlands) and ESEM-JEOL JSM-7600F (JEOL USA Inc., Peabody, MA, USA) in order to observe the microstructure and elemental changes on their surface. Corrosion products formed on AA6061-T6 sample surfaces were identified through X-ray photoelectron spectroscopy (XPS, K-alpha, Thermo Scientific, Waltham, MA, USA). In addition, corrosion products were removed in accordance with ASTM G1-90 standard [33] and the alloy surfaces were reexamined.

2.3. Electrochemical Tests

A multiport electrochemical cell kit (Gamry Instruments, Philadelphia, PA, USA, 1 L total volume) and a potentiostat (Interface-1000E, Gamry Instruments, Philadelphia, PA, USA) were used for all electrochemical measurements. The experimental setup employed was according to ASTM G199-09 standard [34]: two identical AA6061-T6 working electrodes (WEs) connected to a zero-resistance ammeter (ZRA) and a saturated calomel electrode (SCE, $\text{Hg}^{2+}/\text{Hg}_2\text{Cl}_2 = 0.244 \text{ V}$, CH Instruments Inc., Austin, TX, USA) as reference electrode. The electrodes were immersed in an electrochemical cell with seawater, employed as the test electrolyte. All tests were carried out in laminar and stationary (no flow) conditions up to 30 days. Electrochemical noise (EN) data of current and potential fluctuations were collected at different times for 3 h: initial, 1, 5, 15, and 30 days in open circuit potential, OCP, with a sampling frequency of 10 Hz. The obtained data were plotted vs. time. The current fluctuations were considered as electrochemical current noise (ECN) and processed in the frequency domain by fast Fourier transform (FFT) to graph power spectral density (PSD). The PSD as a function of low frequencies was analysed on a bi-logarithmic scale (10^{-3} –1 Hz) of power per unit frequency (A^2/Hz) vs. frequency (Hz). These procedures allowed the fitting of a straight line and obtention of the β slope. The β value characterises the corrosion mechanism on AA6061-T6 surface. The processing of data was realised with Electrochemical Signal Analyzer V.7.0.1 software (Gamry Instruments, Philadelphia, PA, USA). All measurements were checked in triplicate.

Energy Spectral Density

The energy spectral density expresses how the energy of a time series is dispersed with frequency; it can reflect the change in system dynamic. For a signal $X(t)$, the energy E is as follows [35]:

$$E = \int_{-\infty}^{\infty} |x(t)|^2 dt \quad (2)$$

For signals with a finite total energy, an equivalent expression for the energy is expressed as follows:

$$E = \int_{-\infty}^{\infty} |x(t)|^2 dt = \int_{-\infty}^{\infty} |\hat{x}(f)|^2 df \quad (3)$$

It uses the Fourier transform of the signal:

$$\hat{x}(f) = \int_{-\infty}^{\infty} e^{-2\pi ift} x(t) df \quad (4)$$

where f is the frequency in Hz.

The integral on the right-hand side of Equation (3) is the energy of the signal, and the integrand $\left| \hat{x}(f) \right|^2$ describes the energy per unit frequency contained in the signal (ESD).

3. Results and Discussion

3.1. Surface Analysis

Figure 1 shows SEM images of the as-received specimen of 6061-T6 aluminum alloy surface. Small precipitates (labeled as A–C) may be seen (Figure 1b). In accordance with EDS, presented in Table 1, these precipitates correspond to particles rich in Fe and could be considered as elements of the following phases: Al_3Fe , Al–Si–Mn–Fe, and $\alpha\text{-Al}(\text{Fe}, \text{Mn}, \text{Cu})$ [9,10,36]. The elemental composition of the surface layer is indicated by zone D.

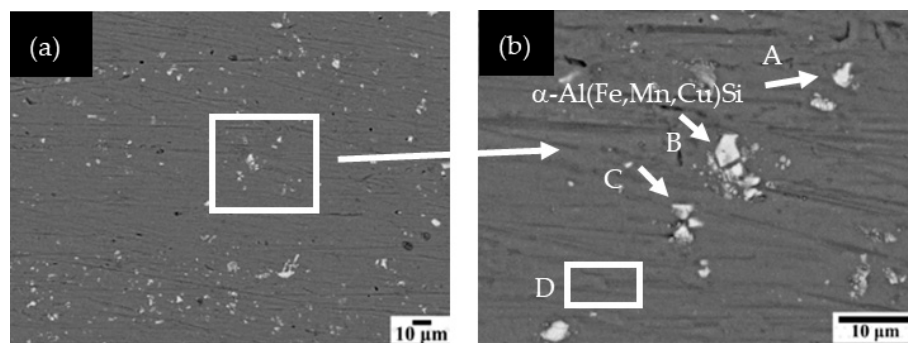


Figure 1. (a) SEM images ($\times 500$) of AA6061-T6 surface before immersion in Caribbean seawater and (b) zoom zone ($\times 2000$).

Table 1. EDS analysis (wt.%) of reference aluminum alloy 6061-T6 surface.

Element	C	O	Mg	Al	Si	Cr	Mn	Fe	Cu
A	2.4	3.3	-	60.3	6.5	1.3	1.6	23.7	0.9
B	2.3	2.7	-	59.3	7.4	1.3	1.5	24.2	1.3
C	2.2	4.5	-	71.7	4.8	0.6	0.9	14.6	0.7
D	2.0	2.1	1.7	93.7	0.5	-	-	-	-

Figure 2a presents the SEM image of the film formed on the surface of the sample after 5 days of immersion in seawater from the Cozumel Channel under laminar flow. It can be clearly seen that the passive layer begins to break down around the alloying elements (Figure 2b). Probably, this layer is less protective in the vicinity of the intermetallic particles, causing the formation of local electrochemical cells with the Al matrix. EDS analysis (Table 2) confirmed the presence of particles mentioned above. According to EDS (Table 2), zone A is characterised by its higher content of Al, O, and Cl, which could relate to corrosion products. According to previous studies, at $\text{pH} > 8.5$, $\text{Al}(\text{H}_2\text{O})_6^{3+}$ cations appear, while in the range of $\text{pH} 4.5\text{--}8.5$, $\text{Al}(\text{OH})_3$ predominates [37,38]. In chloride solutions, aluminum metal ionises rapidly to the Al^{3+} ion, which also hydrolyzes very rapidly (owing to the negative potential value) [39]. Both of these Al cations can react with chloride ions and form AlCl_3 soluble in water (31.77 wt.%) [40]; this is converted later to a relatively stable species of basic aluminum chloride

($\text{AlCl}_3 \cdot \text{H}_2\text{O}$) and transformed slowly to $\text{Al}(\text{OH})_3$ and finally to $\text{Al}_2\text{O}_3 \cdot \text{H}_2\text{O}$, an important corrosion product for the repassivation process of the aluminum surface [39].

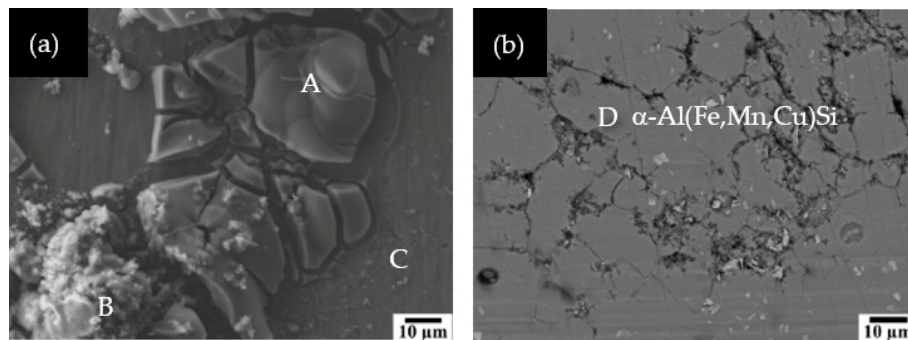


Figure 2. SEM images of AA6061-T6 surface after exposure in Caribbean seawater under laminar flow for 5 days (a) and after removal of corrosion layer (b).

Table 2. EDS analysis (wt.%) of aluminum alloy 6061-T6 surface after 5 days of exposure (zone A, B, C) in Caribbean seawater under laminar flow at 21°C; zone D - after removal of corrosion products.

Element	C	O	Na	Mg	Al	Si	Cr	S	Mn	Cl	K	Ca	Fe	Cu
A	-	47.4	0.7	1.2	25.11	-	-	1.8	-	23.3	-	0.5	-	-
B	6.4	56.6	1.9	1.0	29.2	-	-	0.4	-	0.5	0.5	3.5	-	-
C	4.4	11.5	-	0.8	81.2	0.4	-	0.4	-	0.3	0.8	0.2	-	-
D	10.9	4.7	-	0.4	58.0	5.8	0.6	-	1.2	-	-	-	17.6	0.8

Based on EDS analysis, in zone B, in addition to oxygen and aluminum, elements of calcium and carbon were present, both possibly as a part of a CaCO_3 precipitate originating from seawater. Meanwhile, the layer in zone C maintained a composition similar to that of the alloy, which indicates that the corrosion process was still beginning on the surfaces of similar areas.

After removal of the layer of corrosion products (Figure 2b), an area damaged by pitting and cracking was observed on the alloy surface. However, some precipitates remained on the surface of AA6061-T6, which according to EDS (Table 2) correspond to cathodic particles rich in Fe, $\alpha\text{-Al}(\text{Fe},\text{Mn},\text{Cu})\text{Si}$, that promoted the preferential dissolution of the aluminum matrix (local alkalisiation) [10].

Figure 3 compares SEM images of the aluminum alloy 6061-T6 after exposure at 30 days in laminar flow (Figure 3a,c) and stationary flow (Figure 3b,d). In these micrographs, the products formed on the surfaces of the alloy (Figure 3a,b) can be seen and compared; EDS analysis is summarised in Table 3. In laminar flow (Figure 3a), the segregation of particles rich in Cu (particles A) with the presence of O and Al could be considered as the phases of Al_2Cu , AlMgSiCu (Q-phase), and $\text{Al}_7\text{Cu}_2\text{Fe}$, both relatively resistant to corrosion because they are nobler than the aluminum matrix [4,13]. Q-phase acts as a cathode and does not contribute to intergranular corrosion when it is not connected to any other Cu particle. Otherwise, the Q-phase as cathode promotes the development of intergranular corrosion, initiated in the presence of chloride ions (NaCl). In the corrosion layer, particles without Cu appeared (particles B), rich in Fe, Al, and Mg, which could be attributed to the following phases: Al-Si-Mn-Fe and Al-Mg-Si, reported for aluminum alloy series 6xxx [36]. Zone C of the layer formed under stationary flow (Figure 3b) presented a similar composition of the alloy (Table 3), however, with the oxide layer of $\text{Al}_2\text{O}_3 \cdot \text{H}_2\text{O}$ on the alloy surface 6061-T6, as a transformation product of basic aluminum ($\text{AlCl}_3 \cdot \text{H}_2\text{O}$) in the presence of NaCl [39]. This layer is part of the entire surface (Figure 3a), since the three zones (A–C) have a high oxygen content (Table 3) [4].

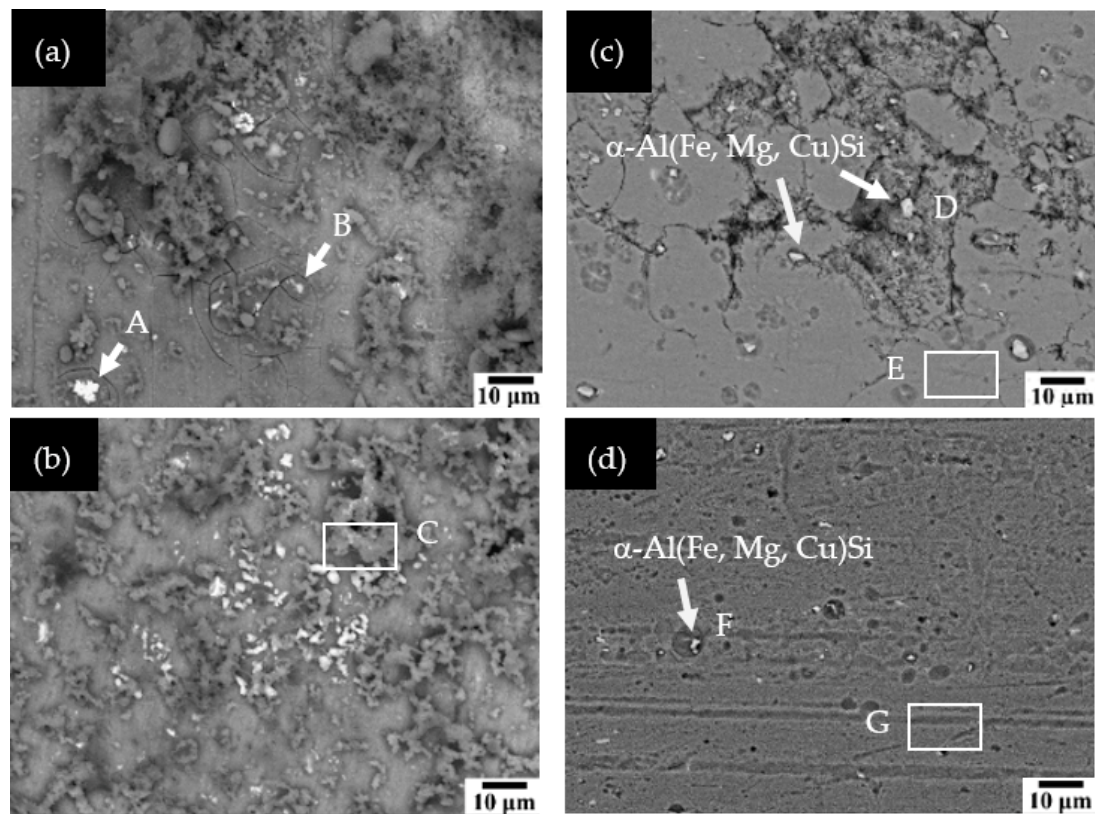


Figure 3. SEM images of AA6061-T6 surface after 30 days of exposure in Caribbean seawater for (a) laminar and (b) stationary flow conditions and after removal of corrosion products for (c) laminar and (d) stationary flow conditions.

Table 3. EDS analysis (wt.%) of aluminum alloy 6061-T6 surfaces: after 30 days of exposure in seawater under laminar flow (zones A, B, C) and after removal the layer of corrosion products (zones D, E, F, G).

Element	C	O	Na	Mg	Al	Si	Cr	Mn	Cl	Ca	Fe	Cu
A	3.3	22.3	2.2	3.3	10.2	0.7	-	-	1.0	0.3	1.0	55.7
B	4.2	31.3	1.7	1.8	39.6	3.9	0.5	0.8	0.8	0.5	14.2	0.7
C	12.7	44.9	0.5	3.0	37.8	0.1	-	-	0.5	0.5	-	-
D	4.1	-	-	-	63.3	6.0	1.0	1.2	1.5	-	21.8	1.1
E	5.7	4.4	-	0.5	84.6	3.2	0.7	0.9	-	-	-	-
F	5.7	1.5	-	-	69.6	5.1	1.3	1.0	-	-	15.0	0.8
G	5.8	4.6	-	0.7	88.2	0.4	0.2	-	-	-	-	-

Figure 3c corresponds to the SEM image of the aluminum alloy 6061-T6 exposed in seawater at 30 days with flow after removal of the layer of corrosion products. An area on the surface damaged by cracking and fissures can be observed, while the surface exposed to seawater without flow (Figure 3d) shows less damage, with pitting holes of several diameters. In contrast, on the surface exposed to laminar flow for this same time period, the pits are not clearly observable, but localised corrosion damage appeared in the form of fissures. This effect is due to the seawater flow, which facilitates the oxygen diffusion and its renewal at the metal interface, accelerating the corrosion process. Moreover, the seawater flow attributes to the detachment of the destroyed passive layer and the appearance of new “fresh” areas, where the oxygen diffuses at the cathodic sites, as an oxidising agent needed for the cathodic corrosion reaction. It is also observed that, on both surfaces (Figure 3c,d), some particles remained (named as D and F), and according to EDS (Table 3), they correspond to cathodic rich in Fe [7], reported in the reference sample as α -Al(Fe,Mn,Cu)Si [36]; these intermetallic particles promoted the preferential dissolution of the aluminum matrix [41,42].

3.2. OCP (Free Corrosion Potential, φ_{corr}) Measurements

Figure 4 compares the φ_{corr} fluctuations of AA6061-T6 specimens exposed for different periods of times (0, 5, and 30 days) under laminar flow conditions (Figure 4a) and without flow (Figure 4b). The average values are summarised in Table 4. The trends in the changes towards more or less negative values are a response to the transformations that have occurred on the surface of the aluminum alloy with the advance of the corrosion process. These are, in the morphology, elemental composition of the layers formed as well as the type of localised corrosion attack discussed previously. It can be seen (Table 4) that the initial values of φ_{corr} are relatively similar, being 30 mV nobler with respect to the exposed surface in laminar flow. At 5 days, which implies the initial destruction of the passive layer (Figure 2a), it is 100 mV more negative with laminar flow than under stationary flow. At 30 days, the φ_{corr} values in both seawater conditions (with and without laminar flow) are very similar (Table 4). However, when the product layer was removed (Figure 3c,d), the SEM images revealed a greater localised attack on the aluminum surface under laminar flow (Figure 3c), while in the absence of flow, this attack has been less aggressive, presenting shallow pits. Free corrosion potential tendency towards more or less negative values indicates periods of corrosion activation or repassivation of the surface, both facts related to the characteristics of the layers formed [4,43].

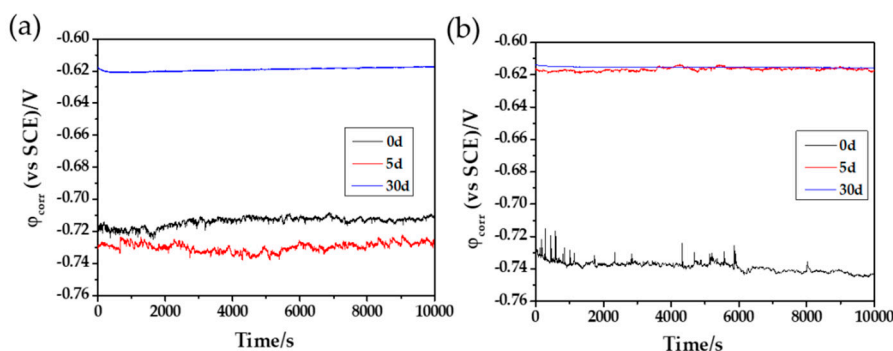


Figure 4. Free corrosion potential (φ_{corr}) values of AA6061-T6 samples in Caribbean seawater during 30 days: (a) with laminar and (b) stationary flows.

Table 4. Average of free corrosion potential (φ_{corr}) values for AA6061-T6 in Caribbean seawater under laminar and stationary flows at different times.

Exposure Time/Days	φ_{corr} vs SCE/mV (Laminar Flow)	φ_{corr} vs SCE/mV (Stationary Flow)
0	-713 ± 2.80	-741 ± 16.40
5	-729 ± 2.70	-619 ± 0.95
30	-618 ± 1.00	-614 ± 0.28

3.3. Surface Characterisation by XPS

In order to identify the composition of the corrosion product layer created on the alloy surface after 30 days of exposure in laminar flow, XPS analysis was carried out on the specimen immersed, taking into account that aluminum corrosion products were not provided by XRD analysis as crystalline phases and are possibly amorphous.

Figure 5a shows the full XPS spectrum of the corrosion products formed on the aluminum alloy surface of 6061-T6. The XPS spectrum revealed signals of Mg, Na, O, Cl, C, Si, and Al, which accord with EDS analysis. The signal of O1s (Figure 5b) centered in 531.88 eV could be attributed to aluminum oxide (Al_2O_3), an important product of the repassivation process of the aluminum surface. The high-resolution peak for Al2p (Figure 5c), situated at 74.38 eV, has been associated with the presence of aluminum hydroxide [$\text{Al}(\text{OH})_3$] [44], possibly derived from the transformation of basic aluminum chloride ($\text{AlCl}_3 \cdot \text{H}_2\text{O}$) [39].

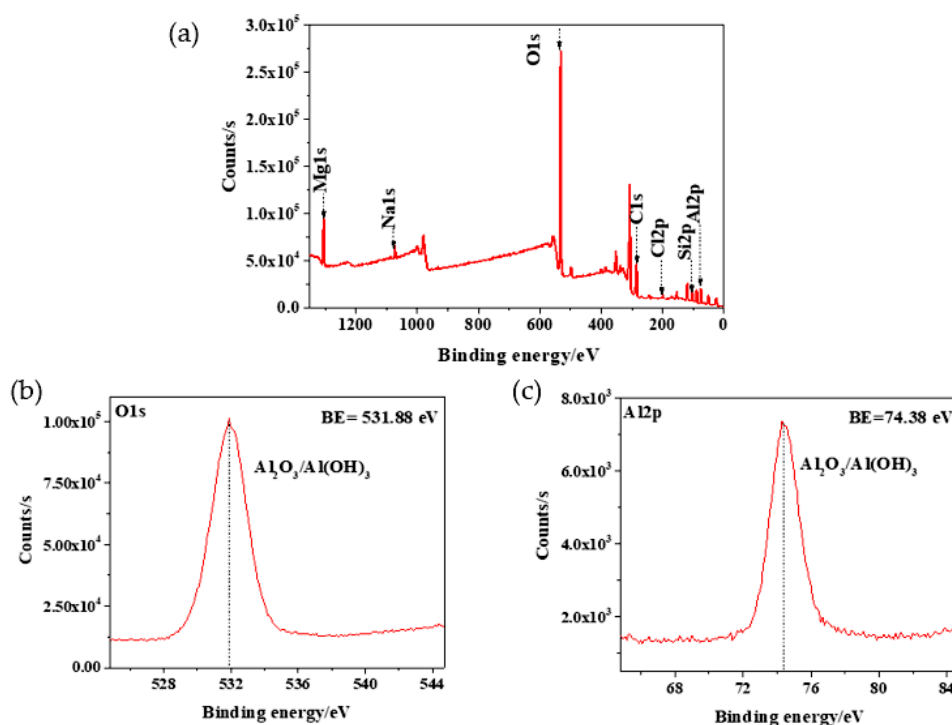


Figure 5. Overview XPS spectra acquired from AA6061-T6 after 30 days of immersion in Caribbean seawater with laminar flow: (a) full spectrum; (b) and (c) spectrum for O1s and Al2p, respectively.

3.4. Electrochemical Current Noise Measurement (ECN)

Figure 6 shows the current oscillations, and it can be seen that, at the beginning of the experiment (0 days), the current density of AA6061-T6 surface immersed in laminar flow of seawater is higher in approximately $50 \mu\text{A cm}^{-2}$ than that current in stationary flow. This suggested that the corrosion of the aluminum alloy 6061-T6 surface in laminar flow initiates faster, when the oxide layer on the alloy begins to break down. However, at the end of the experiment (30 days), the current value diminished suddenly compared with the initial values. However, in stationary flow, the current shifted to one order higher values than those in laminar flow, suggesting an acceleration of the corrosion process at that time [45]. Conversely, the current oscillations in stationary conditions (Figure 6b) presented slow variations, while for flow conditions (Figure 6a), intense current fluctuations were acquired with greater amplitude, which suggest greater corrosion [46]. The observed current oscillations registered in ($\mu\text{A cm}^{-2}$) (Figure 6) correspond to the variation of the free corrosion potential (φ_{corr}) values in several mV (Figure 4).

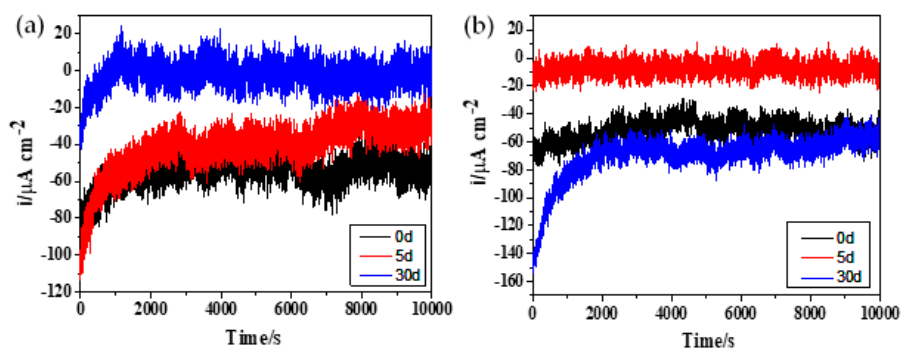


Figure 6. Current density fluctuation for AA6061-T3 immersed in Caribbean seawater up to 30 days under (a) laminar and (b) stationary flows.

The corrosion current density was calculated from the value of polarisation resistance R_p (on the assumption that R_p is equivalent to polarisation resistance noise R_n) obtained by ECN tests, according to the Stern–Geary equation (Equation (5)). R_n is calculated by dividing the standard deviation of potential by standard deviation of current. (The potential noise can be modeled as the action of the current noise on the metal-solution impedance):

$$i_{corr} = \frac{B}{R_p} = \frac{1}{R_p} \times \frac{b_a b_c}{2.303 (b_a + b_c)} \quad (5)$$

where R_p is the polarisation resistance, and b_a and b_c are the Tafel coefficients. In this research, the B value employed was 0.26 V, taking common values for b_a and b_c of aluminum alloys [47,48]. The calculated values (Table 5) show that the corrosion current of AA6061-T6 increases with the time of exposure, being more than one order higher when the alloy is exposed under laminar flow of seawater, while in stationary conditions, it maintains almost similar values up to 30 days.

Table 5. Polarisation resistance (R_p) and corrosion current density values for AA6061-T6 immersed up to 30 days in Caribbean seawater with laminar and stationary flows.

Time/d	$R_p/k\Omega \text{ cm}^2$		$i_{corr}/\mu\text{A cm}^{-2}$	
	Laminar Flow	Stationary Flow	Laminar Flow	Stationary Flow
0	3.65	23.46	7.12	1.11
5	2.24	17.5	11.60	1.49
30	1.44	19.3	18.08	1.35

Subsequently, Faraday’s law was applied to calculate the corrosion rate (CR, Table 6) in the following form:

$$CR = \frac{i_{corr} K E_w}{\rho A} \quad (6)$$

where E_w stands for the equivalent mass of AA6061-T6, i_{corr} is the corrosion density (A cm^{-2}), ρ is the metal density, K is a constant ($3272 \text{ mm/A cm year}$), and A is the exposed specimen area (1 cm^2) [49].

Table 6. Corrosion rate of AA6061-T6 in Caribbean seawater from the Cozumel Channel under laminar and stationary flows.

Time/d	CR/mm year ⁻¹	
	Laminar Flow	Stationary Flow
0	0.08	0.012
5	0.13	0.016
30	0.20	0.014

The corrosion rate values presented in Table 6 indicate that, under laminar flow, the values varied 0.08 and 0.20 mm per year while, in stationary conditions, they were between 0.012 and 0.162 mm per year.

With the statistical data obtained from the corrosion current, the pitting index (PI) [20] was calculated in order to reveal AA606-T6 susceptibility to localised corrosion for the laminar and stationary:

$$PI = \sigma_i (i_{rms})^{-1} = (639.17 \text{ nA}) (666.42 \text{ nA})^{-1} = 0.96 \quad (7)$$

where σ_i is the standard deviation and i_{rms} the main square root of current noise.

Values of PI above 0.1 may indicate localised corrosion [21,50]. The pitting indexes are shown in Table 7. Thus, the calculated PI value suggests that, at the end of the experiment (30 days), for both flow cases, AA606-T6 showed pitting corrosion approximately four times higher in flow conditions, reaching $PI = 0.96$. These facts agree with the SEM images (Figure 3) comparing the corrosion attacks on AA6061-T6 exposed to both flow conditions.

Table 7. Pitting index of AA6061-T6 immersed for 30 days in Caribbean seawater (Cozumel Channel) under laminar and stationary flows.

Time/d	σ_i/nA		i_{rms}/nA		Pitting index	
	Laminar	Stationary	Laminar	Stationary	Laminar	Stationary
0	772	639	5462	5255	0.14	0.12
5	1279	1146	4252	2866	0.30	0.40
30	639	1471	666	6733	0.96	0.22

The current fluctuations, considered as ECN, were transformed into the frequency domain to estimate PSD slopes (β exponent). Figure 7 compares the PSD plots in bi-logarithmic scale, corresponding to AA6061-T6 surfaces after 30 days of exposure in seawater under laminar and stationary flows. In each case, the β exponent decreases as the frequency increases, and this fact could be associated with the advance of the localised corrosion attacks on the alloy surface [35]. At 30 days, β values are similar in laminar and stationary flows (1.0 and 0.94, respectively) and may be attributed to the fractional Gaussian noise (fGn), associated with a persistent process [27]. This type of noise (fGn) is considered also as a stationary process [25].

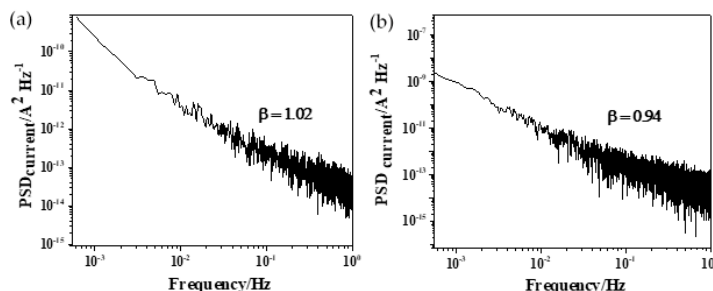


Figure 7. PSD plot (A^2/f) of current noise signal vs frequency (Hz) for AA6061-T6 after 30 days of exposure to seawater: (a) with laminar and (b) stationary flows.

Figure 8 shows the spontaneous energy E during the corrosion process. At the beginning, after 5 days, the energy was of an order of magnitude higher in laminar flow (1.1×10^{-4}). This fact is consistent with the SEM image presented in Figure 2, which showed the accelerated corrosion process causing severe damage to the alloy surface exposed to laminar flow.

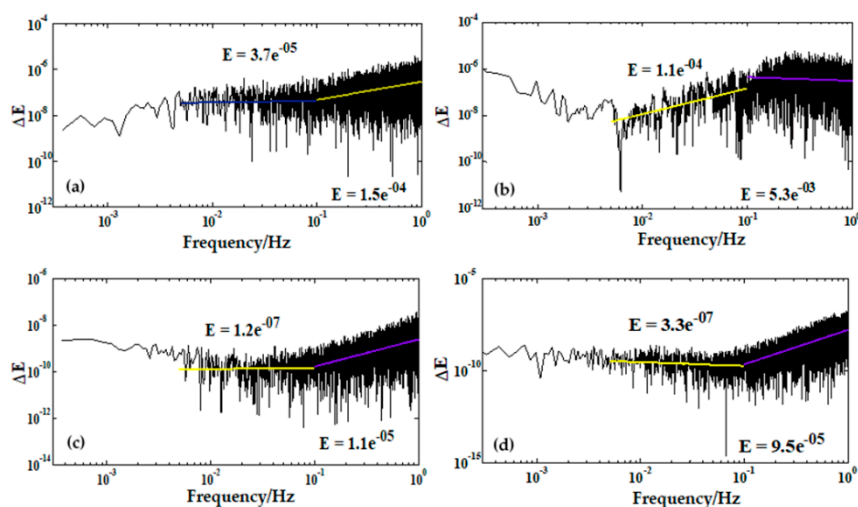


Figure 8. Energy (E) from AA6061-T6 surface after immersion in seawater under laminar flow (a) at 5 days and (b) after 30 days of exposure and stationary flow (c) at 5 days and (d) after 30 days of exposure.

However, at the end of the experiment (30 days), the energy diminished in magnitude, being very similar in the order of 10^{-7} , for both flows probably on account of the formation of layers of corrosion products with different characteristics that act as a physical barrier on the alloy surfaces, slowing down the corrosion attack.

4. Conclusions

1. The initial electrochemical activity of 6061-T6 aluminum alloy surface, immersed in Caribbean seawater, was studied for 30 days under laminar flow (0.1 m s^{-1} , $21 \text{ }^\circ\text{C}$). The changes in the morphology and elemental composition of the formed layers have revealed localised corrosion (fissures and deep cracks) in the vicinity of intermetallic particles rich in Fe and Cu, which act as cathodes. The attack was less aggressive in stationary (no flow) seawater, with shallow pits occurring on the surface at 30 days of exposure.
2. The calculated values showed that the corrosion current (i_{corr}) of AA6061-T6 increases with the time of exposure more than one order higher when the alloy is exposed under laminar flow of seawater ($7.12\text{--}18.08 \mu\text{A cm}^{-2}$) while, in stationary conditions, it maintains almost similar values ($17.51\text{--}19.32 \mu\text{A cm}^{-2}$). With the statistical data obtained from the corrosion current, the calculated pitting index (PI) revealed that AA606-T6 is four times more susceptible to localised corrosion in seawater under laminar flow (PI = 0.96) compared to that in stationary conditions (PI = 0.22). The estimated PSD slopes (β exponent) of the current fluctuations transformed into the frequency domain revealed that, in laminar and stationary flows ($\beta = 1.0$ and 0.94 , respectively), the electrochemical corrosion may be attributed to the fractional Gaussian noise (fGn), associated with a persistent stationary process.
3. The spontaneous energy release in the initial stages is one order higher in laminar flow ($\Delta E = 1.1 \times 10^{-4}$). However, at the end of the experiment (30 days), the energy diminished in magnitude, being very similar in an order of 10^{-7} , for both flows probably on account of the formation of layers of corrosion products with different characteristics that act as a physical barrier on the alloy surfaces, slowing down the corrosion attack.
4. The observed effect of the laminar seawater flow on the AA6061-T6 corrosion process should be considered as a consequence of the facilitated diffusion of the oxygen at the metal–seawater interface, resulting in specific transformation in the composition of the formed corrosion layers. The presented surface SEM-EDS and XPS analysis agree positively with the results obtained with both nondestructive electrochemical methods.

Author Contributions: G.A. and L.C. performed the corrosion test. L.V. and G.A. discussed the results and wrote the manuscript; J.L.L. contributed in the PSD software. L.V. supervised the project. All correspondence should be addressed to L.V. All authors have read and agreed to the published version of the manuscript.

Funding: This research was funded by Centro Mexicano de Inovaci3n en Energ3a del Oci3ano (CEMIE) grant number (00249795).

Acknowledgments: The authors acknowledge LANNBIO for permitting the use of their facilities as well as M. Sci. Dora Huerta and W. J. Cauich-Ruiz for their technical assistance in data acquisition. Luis Ch3vez gratefully thanks CONACYT for his scholarship as a M.Sci. student at CINVESTAV-IPN.

Conflicts of Interest: The authors declare no conflict of interest.

References

1. Davis, J.R.; David, J.R. *Understanding the Basics*; Davis, J.R., Ed.; ASM International: Materials Park, OH, USA, 2001; pp. 351–416.
2. Altenpohl, D.G. *Aluminum Viewed from within: An Introduction into the Metallurgy of Aluminum Fabrication*; Aluminum-Verlag: D3sseldorf, Germany, 1982; pp. 1–225.
3. Pourbaix, M. *Atlas of Electrochemical Equilibria in Aqueous Solutions*; NACE: Houston, TX, USA, 1974; pp. 168–176.

4. Szklarska-Smialowska, Z. Pitting Corrosion of Aluminum. *Corros. Sci.* **1999**, *41*, 743–1767. [[CrossRef](#)]
5. Tiryakioğlu, M.; Staley, J. Physical metallurgy and the effect of alloying additions in aluminum alloys. In *Handbook of Aluminum*; Totten, G.E., MacKenzie, D.S., Eds.; Marcel Dekker, Inc.: New York, NY, USA, 2003; pp. 81–210.
6. Reboul, M.C.; Baroux, B. Metallurgical aspects of corrosion resistance of aluminium alloys. *Mater. Corros.* **2011**, *62*, 215–233. [[CrossRef](#)]
7. Mutombo, K. Intermetallic Particles-induced pitting corrosion in 6061-T651 aluminium alloy. *Mater. Sci. Forum* **2011**, *690*, 389–392. [[CrossRef](#)]
8. Li, J.; Dang, J.G. A Summary of corrosion properties of Al-rich solid solution and secondary phase particles in Al alloys. *Metals* **2017**, *7*, 84. [[CrossRef](#)]
9. Alodan, M.A.; Smyrl, W.H. Detection of localized corrosion of aluminum alloys using fluorescence microscopy. *J. Electrochem. Soc.* **1998**, *145*, 1571–1577. [[CrossRef](#)]
10. Zheng, Y.; Luo, B.; Bai, Z.; Wang, J.; Yin, Y. Study of the precipitation hardening behavior and intergranular corrosion of Al-Mg-Si alloy with differing Si contents. *Metals* **2017**, *7*, 387. [[CrossRef](#)]
11. Ku, M.-H.; Hung, F.-Y.; Lui, T.-S.; Lai, J.-C. Enhanced formability and accelerated precipitation behavior of 7075 Al alloy extruded rod by high temperature aging. *Metals* **2018**, *8*, 648. [[CrossRef](#)]
12. Davoodi, A.; Pan, J.; Leygraf, C.; Norgren, S. The role of intermetallic particles in localized corrosion of an aluminum alloy studied by SKPFM and integrated AFM/SECM. *J. Electrochem. Soc.* **2008**, *155*, C211–C218. [[CrossRef](#)]
13. Birbilis, N.; Buchheit, R. Electrochemical characteristics of intermetallic phases in aluminum alloys an experimental survey and discussion. *J. Electrochem. Soc.* **2005**, *152*, B140–B151. [[CrossRef](#)]
14. McCafferty, E. Sequence of steps in the pitting of aluminum by chloride ions. *Corros. Sci.* **2003**, *5*, 1421–1438. [[CrossRef](#)]
15. Burstein, G.T.; Liu, C.; Souto, R.M.; Vines, S.P. Origins of pitting corrosion. *Corros. Eng. Sci. Technol.* **2004**, *39*, 25–30. [[CrossRef](#)]
16. Guseva, O.; DeRose, J.A.; Schmutz, P. Modelling the early stage time dependence of localised corrosion in aluminium alloys. *Electrochim. Acta.* **2013**, *88*, 821–831. [[CrossRef](#)]
17. LaQue, F.L. *Marine Corrosion: Causes and Prevention*; John Wiley & Sons, Inc.: Hoboken, NJ, USA, 1975.
18. Al-Fozan, S.A.; Malik, A.U. Effect of seawater level on corrosion behavior of different alloys. *Desalination* **2008**, *228*, 61–67. [[CrossRef](#)]
19. Roberge, P. *Handbook of Corrosion Engineering*; The McGraw-Hill Companies, Inc.: New York, NY, USA, 2000.
20. Dawson, J.L. Electrochemical noise measurement: The definitive in-situ technique for corrosion applications. In *Electrochemical Noise Measurement for Corrosion Applications*; Kearns, J., Scully, J., Roberge, P., Reichert, D., Dawson, J.L., Eds.; ASTM STP 1277; ASTM International: West Conshohocken, PA, USA, 1996; pp. 3–35.
21. Xia, D.H.; Song, S.Z.; Behnamian, Y. Detection of corrosion degradation using electrochemical noise (EN): Review of signal processing methods for identifying corrosion forms. *Corros. Eng. Sci. Technol.* **2016**, *51*, 527–544. [[CrossRef](#)]
22. Jiemin, L.; Yang, X.; Zhu, R.; Zhang, Y. Corrosion and serration behaviors of TiZr_{0.5}NbCr_{0.5}V_xMo_y high entropy alloys in aqueous environments. *Metals* **2014**, *4*, 597–608.
23. Tang, Y.; Dai, N.; Wu, J.; Jiang, Y.; Li, J. Effect of surface roughness on pitting corrosion of 2205 duplex stainless steel investigated by electrochemical noise measurements. *Materials* **2019**, *12*, 738. [[CrossRef](#)] [[PubMed](#)]
24. Roberge, P.R. Quantifying the stochastic behavior of electrochemical noise measurement during the corrosion of aluminum. In *Electrochemical Noise Measurement for Corrosion Applications*; Kearns, J.R., Scully, J.R., Roberge, P.R., Reichert, D.L., Dawson, J.L., Eds.; ASTM STP 1277; ASTM International: West Conshohocken, PA, USA, 1996; pp. 142–156.
25. Eke, A.; Hermán, P.; Bassingthwaighte, J.B.; Raymond, G.M.; Percival, D.B.; Cannon, M.; Balla, I.; Ikrényi, C. Physiological time series: Distinguishing fractal noises from motions. *Pflugers Arch. Eur. J. Phys.* **2000**, *439*, 403–415. [[CrossRef](#)]
26. Delignieres, D.; Ramdani, S.; Lemoine, L.; Torre, K.; Fortes, M.; Ninot, G. Fractal analyses for ‘short’ time series: A re-assessment of classical methods. *J. Math. Psychol.* **2006**, *50*, 525–544. [[CrossRef](#)]

27. Planinšič, P.; Petek, A. Characterization of corrosion processes by current noise wavelet-based fractal and correlation analysis. *Electrochim. Acta* **2008**, *53*, 206–5214. [[CrossRef](#)]
28. López, J.L.; Veleva, L.; López-Sauri, D.A. Multifractal detrended analysis of the corrosion potential fluctuations during copper patina formation on its first stages in sea water. *Int. J. Electrochem. Sci.* **2014**, *9*, 1637–1649.
29. Acosta, G.; Veleva, L.; López, J.L. Power spectral density analysis of the corrosion potential fluctuation of aluminium in early stages of exposure to Caribbean sea water. *Int. J. Electrochem. Sci.* **2014**, *9*, 6464–6474.
30. Acosta, G.; Veleva, L.; López, J.L.; López-Sauri, D.A. Contrasting initial events of localized corrosion on surfaces of 2219-T42 and 6061-T6 aluminum alloys exposed in Caribbean seawater. *Trans. Nonferrous Met. Soc. China* **2019**, *29*, 34–42. [[CrossRef](#)]
31. Mena-Morcillo, E.; Veleva, L.P.; Wipf, D.O. Multi-scale monitoring the first stages of electrochemical behavior of AZ31B magnesium alloy in simulated body fluid. *J. Electrochem. Soc.* **2018**, *165*, C749–C755. [[CrossRef](#)]
32. McCabe, W.L.; Smith, J.C.; Harriott, P. *Unit Operations of Chemical Engineering*, 4th ed.; McGraw Hill: New York, NY, USA, 1985; p. 43.
33. ASTM G1–90. In *Standard Practice for Preparing, Cleaning, and Evaluation corrosion Test Specimens*; ASTM International: West Conshohocken, PA, USA, 1999.
34. ASTM G199–09. In *Standard Guide for Electrochemical Noise Measurement*; ASTM International: West Conshohocken, PA, USA, 2014.
35. Stein, J.Y. *Digital Signal Processing: A Computer Science Perspective*, 2nd ed.; John Wiley & Sons, Inc: New York, NY, USA, 2000; p. 115.
36. Yasakau, K.A.; Zheludkevich, M.L.; Ferreira, M.G.S. Role of intermetallics in corrosion of aluminum alloys. Smart Corrosion Protection. In *Intermetallics Matrix Composites: Properties and Applications*; Mitra, R., Ed.; Woodhead Publishing: Aveiro, Portugal, 2018; pp. 425–462.
37. Li, Y.; Gao, G.; Wang, Z.; Di, H.; Li, J.; Xu, G. Effects of the Mg/Si Ratio on microstructure, mechanical properties, and precipitation behavior of Al–Mg–Si–1.0 wt %–Zn alloys. *Materials* **2018**, *11*, 2591. [[CrossRef](#)]
38. Afzal, S.N.; Shaikh, M.A.; Mustafa, C.M.; Nabi, M.; Ehsan, M.Q.; Khan, A.H. Study of aluminum corrosion in chloride and nitrate media and its inhibition by nitrite. *J. Nepal Chem. Soc.* **2006**, *22*, 26–33. [[CrossRef](#)]
39. Foley, R.T.; Nguyen, T.H. The chemical nature in aluminum corrosion, V. Energy transfer in aluminum dissolution. *J. Electrochem. Soc.* **1982**, *129*, 464–467. [[CrossRef](#)]
40. Brown, R.R.; Daut, G.E.; Mrazek, R.V.; Gokcen, N.A. *Solubility and Activity of Aluminum Chloride in Aqueous Hydrochloric Acid Solutions*; U.S. Dept. of the interior, Bureau of Mines: Washington, DC, USA, 1979.
41. Nikseresht, Z.; Karimzadeh, F.; Golozar, M.A.; Heidarbeigy, M. Effect of heat treatment on microstructure and corrosion behavior of Al6061 alloy weldment. *Mater. Des.* **2010**, *31*, 2643–2648. [[CrossRef](#)]
42. Zhu, Y.; Sun, K.; Frankel, G.S. Intermetallic phases in aluminum alloys and their roles in localized corrosion. *J. Electrochem. Sci.* **2018**, *165*, C807–C820. [[CrossRef](#)]
43. Ghali, E. General, galvanic, and localized corrosion of aluminum and its alloys. In *Corrosion Resistance of Aluminum and Magnesium Alloys: Understanding, Performance, and Testing*; Winston Revie, R., Ed.; John Wiley & Sons: Hoboken, NJ, USA, 2010; pp. 176–214.
44. John, F.M.; William, F.S.; Peter, E.S.; Kenneth, D.B. *Handbook of X-ray Photoelectron Spectroscopy*; Physical Electronics Inc.: Chanhassen, MN, USA, 1992.
45. Loto, C.A. Electrochemical Noise Measurement Technique in Corrosion Research. *Int. J. Electrochem. Sci.* **2012**, *7*, 9248–9270.
46. Malo, J.M.; Velazco, O. Electrochemical noise response of steel under hydrodynamic conditions. In *Electrochemical Noise Measurement for Corrosion Applications*; Kearns, J.R., Scully, J.R., Roberge, P.R., Reichert, D.L., Dawson, J.L., Eds.; ASTM STP 1277; ASTM International: West Conshohocken, PA, USA, 1996; pp. 387–397.
47. Sanchez-Amaya, J.M.; Cottis, R.A.; Botana, F.J. Shot noise and statistical parameters for the estimation of corrosion mechanisms. *Corros. Sci.* **2005**, *47*, 3280–3299. [[CrossRef](#)]
48. Curioni, M.; Cottis, R.A.; Thompson, G.E. Application of electrochemical noise analysis to corroding aluminium alloys. *Surf. Interface Anal.* **2013**, *45*, 1564–1569. [[CrossRef](#)]

49. G102-89. In *Standard Practice for Calculation of Corrosion Rates and Related Information from Electrochemical Measurements*; ASTM International: West Conshohocken, PA, USA, 1994.
50. Eden, D.A.; John, D.A.; Dawson, J.L. *International Patent WO 87/07022*; World Intellectual Property Organization: Manchester, UK, 1987.



© 2020 by the authors. Licensee MDPI, Basel, Switzerland. This article is an open access article distributed under the terms and conditions of the Creative Commons Attribution (CC BY) license (<http://creativecommons.org/licenses/by/4.0/>).